Journal of Luminescence 255 (2023) 119567

Contents lists available at ScienceDirect

Journal of Luminescence

journal homepage: www.elsevier.com/locate/jlumin

Full Length Article

Quantitatively identifying the upconversion luminescence mechanisms of Er^{3+}:$NaYF_4$ nanocrystals in aluminosilicate glass ceramics under femtosecond laser field

Xingqing Xie [a,1], Chengzhi Jin [a,1], Zhen Pan [a,1], Jianguo Wang [a], Lianzhong Deng [a,*], Yunhua Yao [a], Dalong Qi [a], Zhenrong Sun [a], Jianrong Qiu [b], Shian Zhang [a,c,**]

[a] State Key Laboratory of Precision Spectroscopy, School of Physics and Electronic Science, East China Normal University, Shanghai, 200241, China
[b] State Key Laboratory of Modern Optical Instrumentation, College of Optical Science and Engineering, Zhejiang University, Hangzhou, 310027, China
[c] Collaborative Innovation Center of Extreme Optics, Shanxi University, Taiyuan, 030006, China

ARTICLE INFO

Keywords:
Upconversion luminescence
Lanthanide-doped nanocrystals
Ultrashort laser pulse

ABSTRACT

Upconversion luminescence of lanthanide ion doped nanocrystals under ultrashort laser pulse excitation can find significant applications in areas like super-resolution nonlinear microscopic imaging and attracts increasing attention. Though major excitation mechanisms, such as excited state absorption (ESA), energy transfer upconversion (ETU) and multi-photon absorption (MPA), have been analyzed and discussed intensively, quantitative differentiation of their respective contributions with convincing experimental proof has seldom been reported however. Here we report experimental demonstration of a simple but effective way to quantitatively identify simultaneous MPA from other mechanisms like ESA and ETU involved in the Er^{3+} doped $NaYF_4$ nanocrystals in aluminosilicate glass ceramics under femtosecond laser field excitation. Comparative studies using laser pulses of the same spectral bandwidth but different time duration or repetition rate are performed and convincing experimental evidences for their respective contribution weights are obtained. The dependence of the MPA excitation efficiency on the spectral bandwidth of the femtosecond laser pulse is also explored for maximizing the upconversion luminescence yield. And predictions from a theoretical model agree well with experimental observations.

1. Introduction

The upconversion luminescence of lanthanide ion doped luminescent materials have been widely studied due to their applications in a wide range of areas like solid-state lasers, phosphors, bio-sensors and imaging [1–6]. A number of factors determine which mechanisms are involved in the excitation processes, like the dopant species and concentration, host material and structure, excitation source and environment [7–14]. Among all the host materials, fluorides of low phonon energy attract a lot of attention with $NaYF_4$ being one of the most widely used ones [15]. Intensive studies with laser excitation at 980 nm and co-doped Yb^{3+} ions as energy sensitizers have been reported and well reviewed [16]. In terms of bio-applications, the 800 nm laser excitation is more favorable since many biological specimens and water have low absorption coefficients at this wavelength. Overheating of the sample can be minimized and deeper penetration depth can be obtained. In recent years, the lanthanide ion doped luminescence materials under ultrashort laser pulse excitation are attracting attention [17–27]. Ultrashort laser pulses, femtosecond laser pulse in particular, possess broad spectral bandwidth, high peak intensity, and can induce new excitation mechanism via multi-photon absorption (MPA) except those conventional ones like excited state absorption (ESA) and energy transfer upconversion (ETU) [16]. Over the years, though a number of studies have been dedicated to recognizing and analyzing these mechanisms, quantitative identification of their contributions with convincing experimental proof has seldom been reported to our

* Corresponding author.
** Corresponding author. State Key Laboratory of Precision Spectroscopy, School of Physics and Electronic Science, East China Normal University, Shanghai, 200241, China.
E-mail addresses: lzdeng@phy.ecnu.edu.cn (L. Deng), sazhang@phy.ecnu.edu.cn (S. Zhang).
[1] These authors contribute equally to this work.

https://doi.org/10.1016/j.jlumin.2022.119567
Received 17 October 2022; Received in revised form 18 November 2022; Accepted 24 November 2022
Available online 5 December 2022

knowledge.

In this paper, we present experimental studies of quantitatively identifying the upconversion luminescence mechanisms in aluminosilicate glass ceramics containing 1%Er^{3+}:$NaYF_4$ nanocrystals under excitation of 800 nm fs laser pulses. Comparative studies using excitation laser pulses of the same spectral bandwidth but different time duration or repetition rate are performed. The corresponding upconversion luminescence of the sample in the visible range is investigated and analyzed with the help of a fiber spectrometer and a streak camera. The contribution percentages of the MPA (specifically, resonance mediated two-photon absorption, RMTPA), ESA and ETU excitation channels to the green and red upconversion emissions are well identified with convincing experimental proof. The laser spectral bandwidth dependence of the RMTPA excitation efficiency is later explored and the maximal excitation efficiency is obtained with an optimal laser spectral bandwidth. A theoretical RMTPA model is finally introduced to explain the experimental observations.

2. Experimental details

Fig. 1 shows a schematic diagram of our experiment. Femtosecond laser pulse of FWHM bandwidth ~20 nm centered at 800 nm from a Ti-sapphire mode-locked regenerative amplifier (Spitfire, Spectra Physics) is used as the excitation source. Normal repetition rate of the laser pulse is 1 kHz. The laser is first guided into a 4f configuration pulse shaper equipped with a liquid-crystal spatial light modulator (SLM-S320d, Jenoptik). Amplitude modulation of the laser pulse can be conveniently realized by programming the voltages applied on the liquid crystals of the SLM with the combination of a polarizer. The laser exiting the pulse shaper is focused on the sample via a lens of 200 mm focus length and luminescence is collected perpendicularly by a spectrometer (2300i, Princeton Instrument) before being sent to a stream camera (C7700, Hamamatsu). A fiber spectrometer (Maya, Ocean Optics, not shown in the figure) monitors the luminescence over the sample as well.

The sample of 1%Er^{3+}-doped $NaYF_4$ nanocrystals in aluminosilicate glass ceramic was prepared from raw materials of $40SiO_2$–$25Al_2O_3$–$18Na_2CO_3$–$10YF_3$–$7NaF$–$1ErF_3$ (mol.%). The original materials were first melted in a platinum crucible under atmosphere at 1450 °C for about an hour and then cast into a metal mold followed by annealing at 450 °C for about 10 h. The sample was further heat treated to 600 °C for 2 h and cooled to room temperature to form glass ceramics via crystallization. Corresponding XRD curve and TEM images indicated that the cubic α-phase $NaYF_4$ nanocrystals were formed and well distributed in the sample, as those shown in our previous work [28].

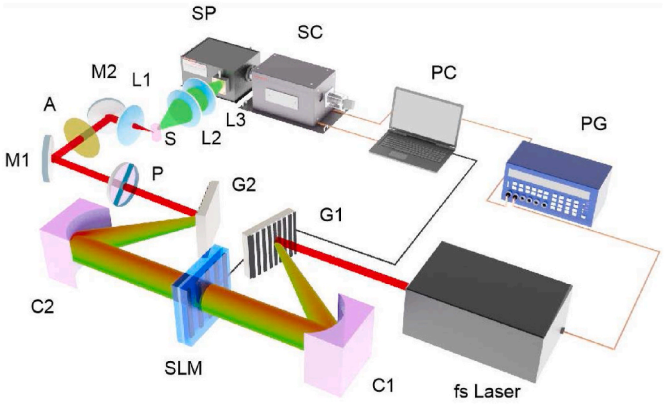

Fig. 1. Schematic diagram of the experiment. C1 and C2: cylindrical concave mirrors; G1 and G2: gratings; SLM: spatial light modulator; P: polarizer; M1 and M2: reflective mirrors; A: attenuator; L1, L2 and L3: focusing lenses; S: sample; SP: spectrometer; SC: streak camera; PC: personal computer; PG: pulse generator.

3. Results and discussion

Absorption spectrum of the sample is first measured with a spectrometer (TU-1901, Purkinje) and presented in Fig. 2(a). Main absorption peaks appearing at wavelengths about 404, 450, 485, 518, 542, 650 and 799 nm correspond to transitions from the ground state $^4I_{15/2}$ to excited states $^2H_{9/2}$,$^4F_{3/2}$, $^4F_{7/2}$, $^2H_{11/2}$, $^4S_{3/2}$, $^4F_{9/2}$ and $^4I_{9/2}$, respectively. The visible upconversion luminescence under excitation of 800 nm fs laser pulses of repetition rate 1 kHz recorded by the Maya fiber spectrometer is given in Fig. 2(b). The laser power is measured to be about 80 mW before the focusing lens and the pulses have a measured time duration of about 50 fs? Five main emission peaks appearing at about 406, 472, 525, 545 and 656 nm are mainly assigned to transitions from states $^2H_{9/2}$,$^4F_{7/2}$, $^2H_{11/2}$, $^4S_{3/2}$ and $^4F_{9/2}$ to the ground state $^4I_{15/2}$. A small peak appearing at about 620 nm is assigned to the transition from state $^4F_{3/2,5/2}$ to state $^4I_{13/2}$. The green (525 and 545 nm) and red emission (656 nm) bands dominate the visible luminescence spectrum. The two peaks appearing at wavelength 406 and 472 nm are also very strong, which are usually indiscernible in conventional experiments with cw or Q-switched laser excitation.

The dependence of the upconversion luminescence intensity (I) on the pump laser intensity (I_P) is also studied. Fig. 3(a) presents the relationship between the measured luminescence intensity and the pump laser intensity in log-log plot. The pump laser power is directly measured using a power meter before the focusing lens. The corresponding laser intensity is determined by estimating the size of the laser focus spot using the conventional formular $d = 4f\,\lambda/\pi/D$, with f being the focal length of the lens, λ and D being the wavelength and size of the incident laser beam. The fitted slopes for the green (solid squares) and red (solid circles) emissions are about 1.90 and 1.74, respectively. According to the conventional relationship of $I \propto I_P^N$, with N being the number of absorbed photons [29], this indicate two photon absorption should be involved in the excitation process. Fig. 3(b) gives the energy structure of the doping Er^{3+} ion, possible excitation mechanisms and luminescence transitions involved. Under broadband 800 nm fs laser excitation, single photon absorption (SPA: $^4I_{15/2}+h\nu \rightarrow {}^4I_{9/2}$) and resonance-mediated two photon absorption (RMTPA: $^4I_{15/2}+2h\nu \rightarrow {}^2H_{9/2}$) via state $^4I_{9/2}$ can occur. Previous studies have recognized that excited state absorption (ESA: ① $^4I_{13/2} + h\nu \rightarrow {}^2H_{11/2}$, ② $^4I_{11/2} + h\nu \rightarrow {}^4F_{3/2}$, ③$^4I_{9/2} + h\nu \rightarrow {}^2H_{9/2}$) and energy transfer upconversion (ETU: ① $^4I_{13/2} + {}^4I_{11/2} \rightarrow {}^4F_{9/2} + {}^4I_{15/2}$, ② 2 $^4I_{11/2} \rightarrow {}^4F_{7/2} + {}^4I_{15/2}$) are major contribution channels for the green and red emissions in conventional experiments with cw or pulsed laser excitation. Since the RMPTA, ESA and ETU processes all involve two photon absorption, therefore they are indistinguishable from each other by simply checking the slopes of the log$I$-logI_P plot and other experimental proof are needed to differentiate them.

Contribution of ETU process is conventionally determined by studying the time evolution of the upconversion luminescence with a rising edge on the time profile of its intensity might be observed [30]. Fig. 4(a) and (b) show the streak camera recorded images of the green and red emissions in both spectral and temporal dimensions under excitation of 1 kHz fs laser pulses. The time profiles of the integrated luminescence intensity from the recorded images are plotted in Fig. 4(c). As one can see, no discernible rising edges (or humps) appear on the time profiles of both emissions. The decay lifetimes, defined here as the time for the normalized signal intensity decaying to its 1/e value just for later comparison, are about 4.5 and 24.0 μs for the green and red emissions, respectively. Considering the 800 nm SPA resulted populations in the lower excited states $^4I_{11/2}$ and $^4I_{13/2}$, the ETU channels mentioned above should make some contributions to the upconversion luminescence. However, the presence of other major contributing channels, like RMTPA and ESA, may prevent the rising edges from being observed, as will be discussed in the following analysis.

Compared to SPA, the contribution of RMTPA is accountable only when the excitation laser intensity is rather high due to the tiny TPA cross section. This high laser intensity demand is usually met only with

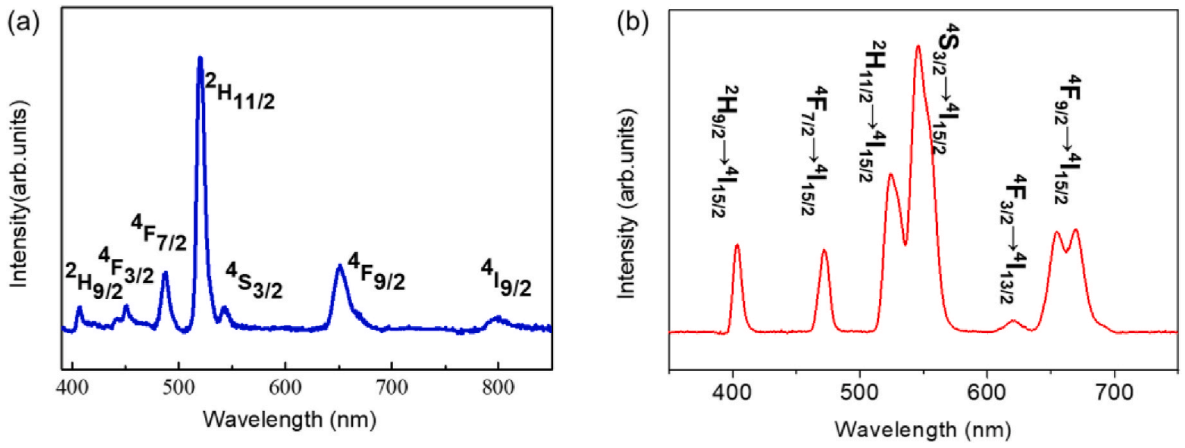

Fig. 2. (a) Absorption spectrum of the sample in the range of interest; (b) upconversion luminescence spectrum under 800 nm fs laser excitation.

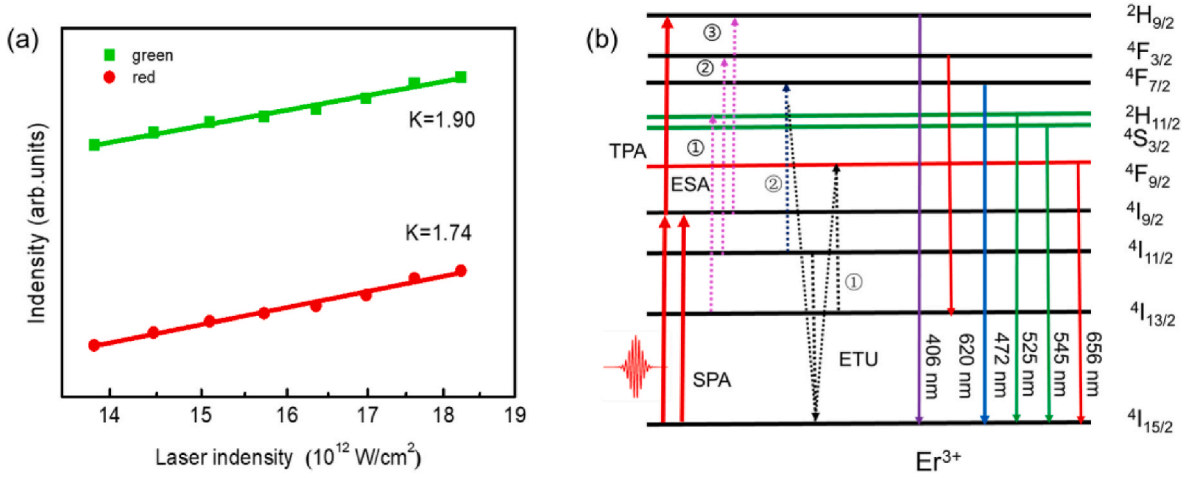

Fig. 3. (a) Laser intensity dependence of the green and red emission intensities; (b) energy level structure of the doping Er^{3+}, possible excitation mechanisms and luminescence transitions involved.

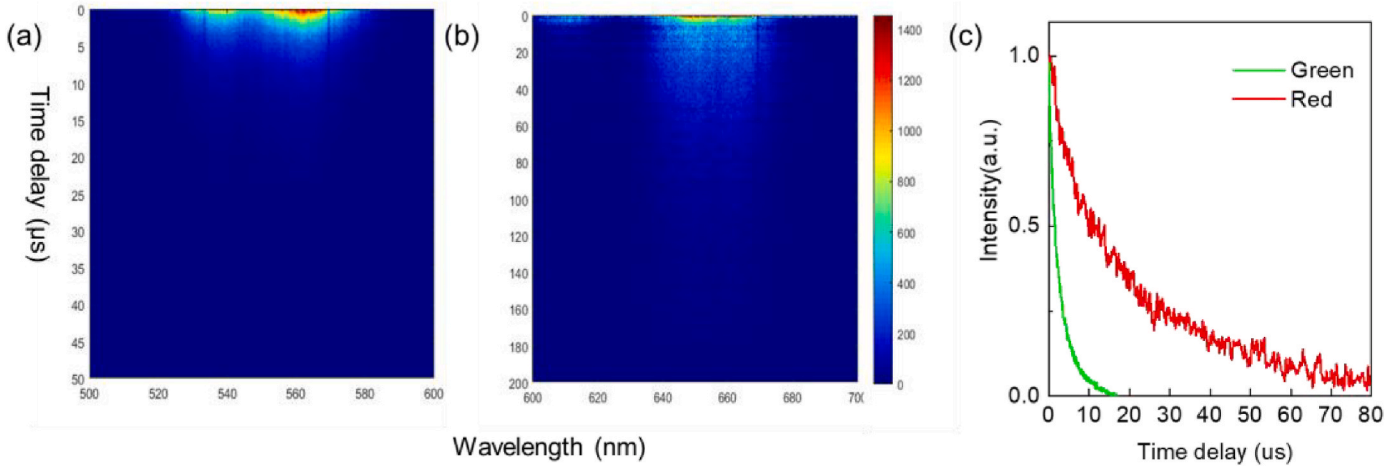

Fig. 4. (a) and (b) Streak camera recorded images, (c) time evolution of the integrated intensities of the green and red emissions, respectively.

Pico- or femtosecond laser pulses. With this in mind we perform a comparative study and irradiate the sample with femtosecond and nanosecond laser pulses of repetition rate 1 kHz, respectively. The nanosecond laser pulse is first obtained from the femtosecond laser amplifier by blocking the mode-locked femtosecond seed pulse and then amplitude modulated by the pulse shaper to have the same spectral profile as the femtosecond pulse (as shown later in Fig. 8(a)). The laser power of both the femtosecond and nanosecond pulses is measured to be about 80 mW before the focusing lens. The time durations (FWHM) of the femtosecond and nanosecond laser pulses are about 50 fs and 50 ns,

respectively. This huge difference in peak laser intensity ensures that the contribution of RMTPA can be safely ignored when nanosecond laser pulses are being used as excitation source.

Fig. 5 shows the upconversion luminescence spectra under excitation of 1 kHz fs (red line) and nanosecond (blue line) pulses, respectively. The upper right inset presents the downshift luminescence peak at wavelength 978 nm, corresponding to state transition $^4I_{11/2} \rightarrow {}^4I_{15/2}$. In fact, the peak intensities at 978 nm are rather close for the two cases even without normalization. This indicates that SPA and downshift luminescence behave much the same way in the two cases. Considering that the femtosecond and nanosecond pulses are the same in spectral profile, this behavior is totally understandable. As one can see, under nanosecond pulse excitation the three signal peaks at 406 ($^2H_{9/2} \rightarrow {}^4I_{15/2}$), 472 ($^4F_{7/2} \rightarrow {}^4I_{15/2}$) and 620 nm ($^4F_{3/2,5/2} \rightarrow {}^4I_{13/2}$) disappear below the background level. The ESA and ETU processes in upconversion excitation should function almost the same way for the two cases, since both femtosecond and nanosecond pulses are short enough compared to the lifetimes of involved excited states $^4I_{9/2}$, $^4I_{11/2}$ and $^4I_{13/2}$, which range from tens of microsecond to a few millisecond [31,32]. This indicates that neither the ESA ② or ③ nor the ETU② channels, as marked in Fig. 3(b), play noticeable roles in exciting populations on higher energy states $^2H_{9/2}$, $^4F_{3/2,5/2}$ and $^4F_{7/2}$. And the disappearance of the three signal peaks is ascribed to the absence of RMPTA contribution since the nanosecond laser pulse intensity is too weak to induce efficient RMPTA here. The area integrated intensity of the green luminescence (525 and 545 nm) is severely reduced to about ~13% of its original value (fs 1 kHz). This 13% contribution should come dominantly from the ESA① channel and slightly from the ETU② channel. And the missing 87% contribution can be mainly ascribed to absence of the RMTPA resulted higher state population followed by multi-phonon relaxation. The intensity of the red emission (656 nm) is however less affected and decreased to only about ~65% of the original value (fs 1 kHz). Similarly, the missing 35% contribution can be mainly ascribed to absence of the RMTPA channel. Since the ETU① channel is hardly affected by the change from femtosecond to nanosecond laser pulses, it is left being the major contributor to the red emission with contribution weight of about ~65%.

For more evidence, Fig. 6 presents the streak camera recorded images of the green (a) and red (b) emissions in both spectral and temporal dimensions under excitation of 1 kHz ns laser pulses. Similarly, the time

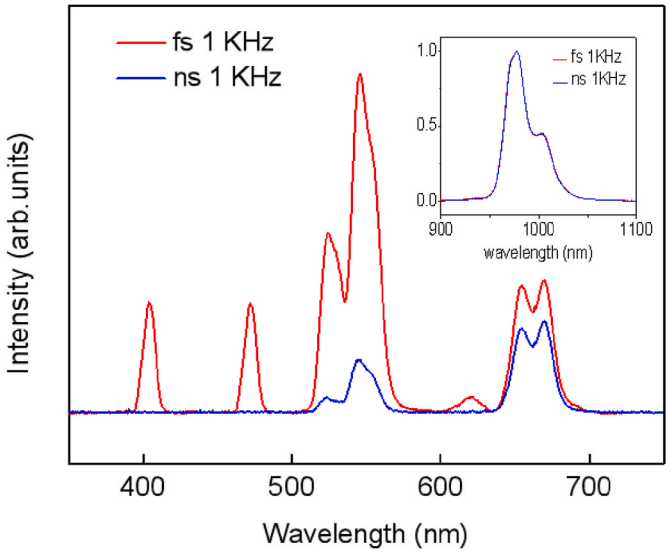

Fig. 5. The upconversion luminescence spectra under excitation of femtosecond (red line) and nanosecond (blue line) laser pulses of 1 kHz, respectively. The inset plots the downshift luminescence peak at wavelength 978 nm (state transition $^4I_{11/2} \rightarrow {}^4I_{15/2}$).

profiles of the integrated luminescence intensity from the recorded images are plotted in Fig. 6(c). The decay lifetimes are about 5.9 and 230.0 μs for the green and red emissions, respectively. As one can see, with the time duration of the excitation pulses extended from femtosecond to nanosecond, the time profile of the green emission remains a similar exponential decay with its lifetime slightly increased from about 4.5 to 5.9 μs; the time profile of the red emission however is totally different with a rising edge appearing, and its decay lifetime is increased from about 24.0 to 230.0 μs? This confirms our above analysis: Under nanosecond laser pulse excitation the ESA① channel rather than the ETU② channel plays a dominant role in exciting the green upconversion luminescence, while the ETU① channel is the major contributor to the red upconversion luminescence. Since ETU① channel is left being the major contributor, the decay lifetime of the red emission gets long. Now, we can explain why there is no discernible rising edge in the time profile of the red emission under femtosecond laser excitation: There are two major excitation channels contributing to the red emission. One is ETU① channel and the other is the RMTPA channel. The ETU① channel contributed red emission begins with a characteristic rising edge followed by a long decay tail. The RMTPA channel contributed red emission, however, decays in a relatively fast exponential way. The RMTPA channel contribution overlaps in time with that of the ETU① channel in its rising edge, and thus prevents the rising edge from being observed (as can be seen in Fig. 4(c)).

Comparative studies are also performed with femtosecond laser pulses of repetition rate 1 kHz and 100 Hz, respectively. Fig. 7 gives the corresponding upconversion luminescence spectra (red line for 1 kHz and blue line for 100 Hz). For the case of repetition rate 100 Hz, the number of laser pulses is reduced by a factor of 10 and thus the time-integrated signal gets rather weak, as shown by the noisy background level from the fiber spectrometer. For better comparison, the spectrum signals are divided by their corresponding repetition rate respectively and normalized at the peak at 406 nm ($^2H_{9/2} \rightarrow {}^4I_{15/2}$). As one can see, the other two peaks 472 ($^4F_{7/2} \rightarrow {}^4I_{15/2}$) and 620 nm ($^4F_{3/2,5/2} \rightarrow {}^4I_{13/2}$) overlap well for both cases. The green peak (525 and 545 nm) is slightly reduced to about ~89% of its original value (1 kHz). The red peak (656 nm) is most affected and reduced to about ~51% of its original value. Considering the noisy background level these two values might be just rough estimations of their real ones, particularly the last one for the red peak. But they still provide helpful information in understanding the mechanisms behind. As discussed above, the three signal peaks at 406, 472 and 620 nm are basically contributed by the RMPTA channel. Contribution from RMPTA channel involves simultaneous absorption of two excitation photons from the same laser pulse and has no relationship with neighboring pulses and thus no dependence on the repetition rate here. The channels of ESA① ($^4I_{13/2} + h\nu \rightarrow {}^2H_{11/2}$), ETU① ($^4I_{13/2} + {}^4I_{11/2} \rightarrow {}^4F_{9/2} + {}^4I_{15/2}$) and ETU② 2 $^4I_{11/2} \rightarrow {}^4F_{7/2} + {}^4I_{15/2}$ channels are however dependent on the populations of the states involved for each laser pulse. The states $^4I_{11/2}$ and $^4I_{13/2}$ involved in the ESA①, ETU① and ETU② channels have lifetimes of a few milliseconds [31,32]. When the laser pulse repetition rate changes from 1 kHz to 100 Hz, the time interval between neighboring laser pulses will be increased from 1 to 10 ms and the populations of the two states will be greatly reduced, particularly that of the state $^4I_{13/2}$ with longer lifetime. Thus, contributions of the ESA①/ETU② and ETU① channels to the green and red emissions will be greatly suppressed. However, the RMTPA channel resulted contributions to the green and red emissions remain about the original values of 0.87 and 0.35, and thus play an even more dominant role with their percentages increased to about 97% (0.87/0.89) and 68% (0.35/0.51), respectively. Unfortunately, the signal intensities of both the green and red emissions under laser pulses of 100 Hz are too weak to produce informative streak camera images for further analysis. One thing worth pointing out is that, for each laser pulse the ESA① channel can only happen with state populations resulted from preceding laser pulses rather than the present one, whose resulted population in the lower state is too late to make contribution. The ETU①/② channels can

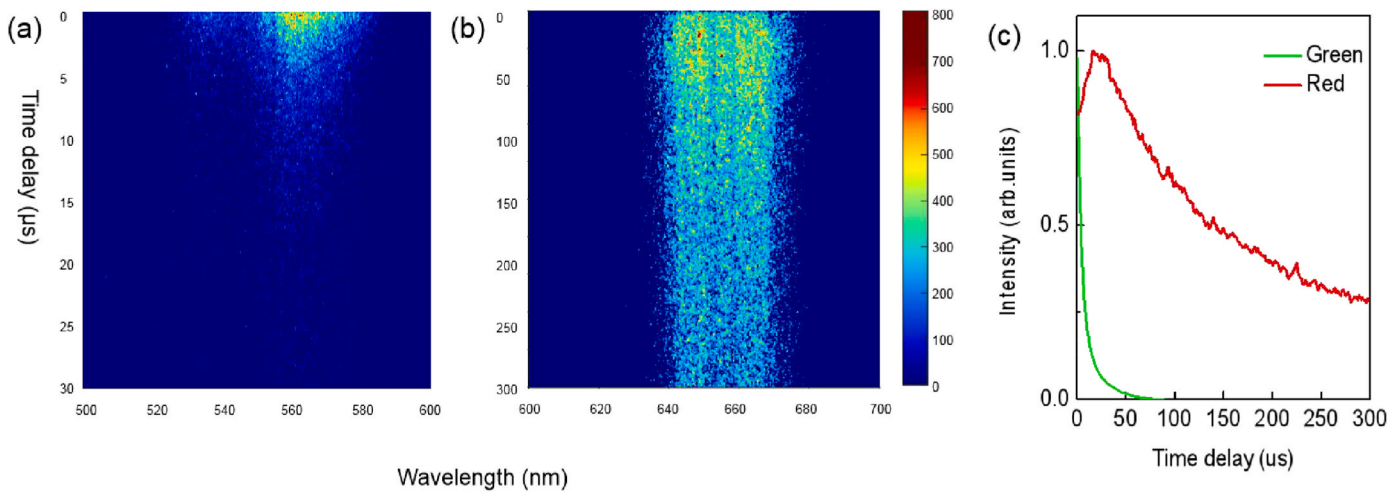

Fig. 6. (a) and (b) Streak camera recorded images, (c) time evolution of the integrated intensities of the green and red emissions, respectively.

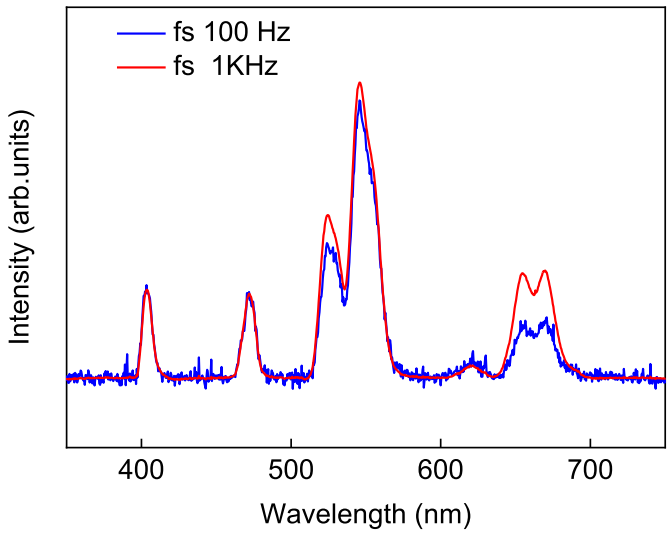

Fig. 7. The upconversion luminescence spectra under excitation of femtosecond laser pulses of repetition rates 1 kHz (red line) and 100 Hz (blue line), respectively.

however make full use of state populations resulted from both preceding and present laser pulses. As the repetition rates changes from 1 kHz to 100 Hz, state populations are mainly induced by the present laser pulse rather than preceding ones. Therefore, compared to the ETU①/②-channels the ESA① channel is more affected by the decrease of repetition rate. As for the influences of Er^{3+} dopant concentration on the contribution weights of the above major excitation channels under femtosecond laser excitation. High dopant concentration can lead to large Er^{3+} ion number density and small ion-ion distance, which are more conducive to ESA and ETU processes and thus help improve their contribution percentages, particularly the highly ion-ion distance dependent ETU channel. Conversely, low dopant concentration will suppress the ESA and ETU excitation channels more and thus help improve the RMTPA channel contribution weight.

The Er^{3+} doped $NaYF_4$ nanocrystals under RMTPA excitation can find significant application in super-resolution microscopic bioimaging when they are contained in nanoparticles [33,34]. Compared to single photon excitation, two-photon excitation demands strong laser intensity and fluorescence can only occur in a tiny volume of the focus spot, in which the laser intensity is strong enough to meet the requirement for two-photon excitation. This well localized fluorescence excitation and emission can offer better spatial resolution for microscopic imaging. Besides, the fluorescence excitation via RMTPA is fulfilled in a time scale of less than picosecond, which is suitable for pump-probe studies of fast dynamic processes taking place in bio-samples. Though femtosecond

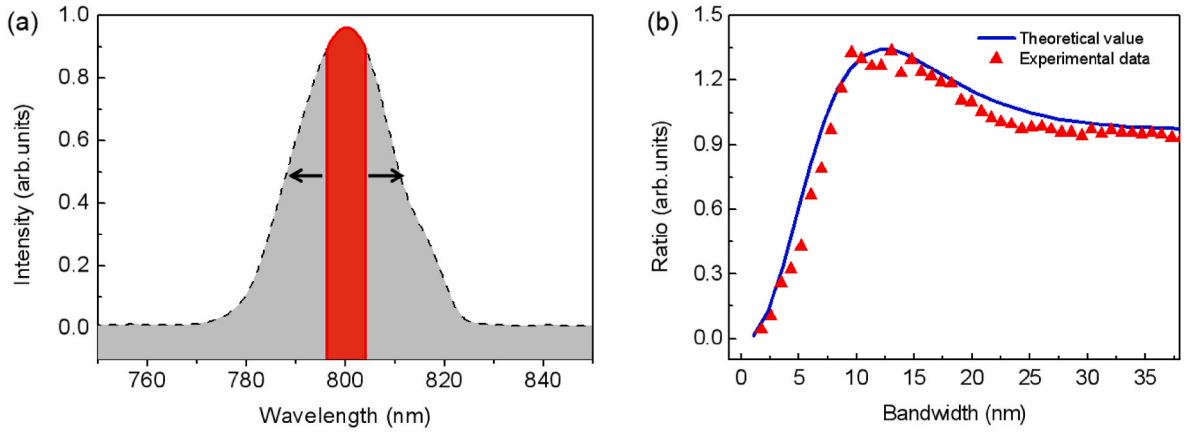

Fig. 8. (a) Tailoring the spectral bandwidth of the laser pulse by amplitude modulating the spectral components: the envelope of the gray area representing the bandwidth of the unshaped laser pulse and the mid red area indicating the spectral components allowed to exit the pulse shaper; (b) the dependence of the ratio on the laser pulse bandwidth: solid triangles and line indicating experimental and theoretical results, respectively.

laser pulses can serve as an ideal light source for multi-photon excitation, the high peak laser intensity is prone to cause optical damage of the sample. In fact, not all the spectral components in the laser pulse make equal contributions in exciting the upconversion luminescence. We wonder how the laser spectral bandwidth affects the excitation efficiency of the luminescent ion. If there exists a maximal excitation efficiency for an optimal laser spectral bandwidth, one can choose to work with it for maximal upconversion luminescence yield while keeping the laser peak power under damage threshold.

For this reason, we proceed to study the laser spectral bandwidth dependence of the RMTPA induced upconversion luminescence efficiency under the 800 nm fs laser pulses of 1 kHz. The spectral bandwidth of the laser pulse is controlled in such a way: starting from the central wavelength at 800 nm, more spectral components at both shorter and longer wavelengths are gradually allowed to exit the pulse shaper via amplitude modulation, and reach the sample, as shown in Fig. 8(a). The glass ceramic sample containing nanocrystals is known to be rather scattering, and the focused laser beam exiting from the sample is seriously deformed due to scattering and other nonlinear interactions with the sample. And a reasonable measurement of the absolute absorption of the excitation photons via conventional absorption techniques is not available. Therefore, we turn to characterize the resonance-mediated two-photon excitation efficiency by measuring the ratio of the green fluorescence emission intensity to the averaged laser power of the femtosecond laser pulses instead. As the pulse bandwidth gets broad step by step, both the values of the area integrated green emission intensity and the power of the transmitted laser spectral components are measured. The ratio of the above two values, taken as a measure of the average laser power dependence of the upconversion luminescence efficiency, is obtained and presented in Fig. 8(b) (solid triangles). As one can see, the optimal excitation efficiency is obtained with a pulse bandwidth of about 12 nm. Keep in mind the corresponding pulse duration in time is now elongated to about 1.7 times the original value of full spectral bandwidth and this helps in reducing the laser pulse peak power further.

To further understand the above observations in experiment, let us turn to the RMTPA transition probability under laser pulse excitation, which can be approximated as [35]

$$P \propto \int_{-\infty}^{+\infty} d\omega_f A(\omega_f) \left| A(\omega_i) \int_{-\infty}^{+\infty} E(t_1) \exp\left[i(\omega_f - \omega_i) t_1 \right] \times \int_{-\infty}^{t1} E(t_2) \exp\left[i(\omega_i t_2) d_{t_2} d_{t_1} d_{\omega_i} \right|^2 \quad (1)$$

where ω_i and ω_f are the resonant transition frequencies from the ground state $|g>$ to the intermediate state $|i>$ and final state $|f>$, $A(\omega_i)$ and $A(\omega_f)$ are the absorption line shape functions of states $|i>$ and $|f>$, and $E(t)$ is the electric field of the laser pulse in time domain. By transforming into the frequency domain, we can approximate the RMPTA transition probability as

$$p \propto \int_{-\infty}^{+\infty} d\omega_f A(\omega_f) |A_R + A_{NR}|^2 \quad (2)$$

with

$$A_R \propto i\pi \int_{-\infty}^{+\infty} d\omega_i E_0(\omega_f - \omega_i) E_0(\omega_i) \times Exp\{ i[\varphi(\omega_f - \omega_i) + \varphi(\omega_i)] \} \quad (3)$$

$$A_{NR} \propto \wp \int_{-\infty}^{+\infty} d\omega E_0(\omega_f - \omega) E_0(\omega) \times Exp\{ i[\varphi(\omega_f - \omega) + \varphi(\omega)] \} \Big/ (\omega_i - \omega) \quad (4)$$

Here A_R represents contributions from all the resonant two-photon absorption via the intermediate state $|i>$ with transition frequencies of ω_i and ω_f-ω_i, and A_{NR} represents contributions from all the near-resonant two-photon absorption not via the intermediate state $|i>$ with transition frequencies of ω and ω_f -ω. $E(\omega) = E_0 \times Exp[i\varphi(\omega)]$ is the Fourier transform of$E(t)$ with E_0 and $\varphi(\omega)$ being the spectral amplitude and phase respectively, $\wp$ is the Cauchy's principal value to exclude the on-resonance transitions.

Different from gaseous atoms with rather narrow absorption linewidth [35], the lanthanide ions doped in crystals possess broad absorption bandwidth and a huge number of excitation pathways can interfere. Depending on the relative phases of the spectral components, constructive or destructive interference can occur. Based on the above equations the ratio of the RMTPA transition probability to the laser pulse power as a function of spectral bandwidth is numerically calculated. The solid line in Fig. 8(b) presents the calculated results for the doping Er^{3+} ion. The wavelengths for the intermediate and final states involved in theoretical RMTPA calculation are centered at 799 and 404 nm respectively, corresponding to absorption from the ground state $^4I_{15/2}$ to excited states $^4I_{9/2}$ and $^2H_{9/2}$, as shown in Fig. 2(a). As one can see, theoretical results well reproduce the experimental observations.

4. Conclusion

In summary, comparative studies using excitation laser pulses of the same spectral bandwidth but different time duration or repetition rate have been performed for the first time to provide convincing evidences for differentiating the excitation mechanisms and their contribution weights involved in the 1%Er^{3+} doped $NaYF_4$ nanocrystals contained in aluminosilicate glass ceramics. With femtosecond laser pulses of 1 kHz, the RMTPA channel can contribute ~87% and ~35% to the green and red upconversion luminescence, respectively. It is also found that even though the ETU channel makes a major contribution of ~65% to the red luminescence, there is no discernible rising edge in the time profile of the signal intensity. This is because the fast exponentially decayed RMTPA contribution happens to concentrate on the rising edge of the ETU channel resulted signals. As the laser pulse repetition rate is reduced to 100 Hz, contributions from the ESA and ETU channels are severely suppressed due to the decreased state populations involved, the RMTPA channel however functions the same with its contribution weights to the green and red emissions increased to about 97% and 68%, respectively. The comparative studies presented here demonstrate a simple but effective way to quantitatively differentiate simultaneous MPA from other mechanisms like ESA or ETU involved in upconversion luminescence of doped lanthanide ions. In addition, the laser spectral bandwidth dependence of the RMTPA excitation efficiency for upconversion luminescence is also explored. Experimental results indicate that the maximal laser power excitation efficiency can be obtained with a laser spectral bandwidth of about 12 nm for the sample under study. Theoretical predictions from a RMTPA model are consistent with the experimental observations. In real applications like nonlinear microscopic imaging, maximizing the quantum yield of the weak MPA induced upconversion luminescence while keeping the sample optically safe is always desirable. This study demonstrates a feasible way of optimizing the laser spectral bandwidth to maximize the MPA excitation efficiency and thus the upconversion luminescence yield. Though the results presented here might be unique to the experimental conditions and sample under our study, the method demonstrated and the phenomena observed are of general reference value to other lanthanide ion doped luminescent materials under ultrashort laser pulse excitation.

Author contributions

Conceptualization, L. Deng, S. Zhang; material preparation, J. Qiu; data acquisition, X. Xie, C. Jin, Z. Pan, J. Wang; data analysis, X. Xie, C. Jin, Z. Pan; writing - original draft, X. Xie, L. Deng, review and editing, L. Deng, Y. Yao, D. Qi, Z. Sun, J. Qiu, S. Zhang; Funding acquisition, L. Deng, Y. Yao, D. Qi, Z. Sun, S. Zhang.

Declaration of competing interest

The authors declare that they have no known competing financial interests or personal relationships that could have appeared to influence the work reported in this paper.

Data availability

Data will be made available on request.

Acknowledgements

This work was partially supported by the National Natural Science Foundation of China (Grant Nos. 91850202, 92150301, 12074121, 62105101, 62175066, 11727810, 12034008), the Science and Technology Commission of Shanghai Municipality (Grant Nos. 21XD1400900, 20ZR1417100, 21JM0010700).

References

[1] H. Zhou, M. Wissinger, J. Fallert, R. Hauschild, F. Stelzl, C. Klingshirn, H. Kalt, Ordered, uniform-sized ZnO nanolaser arrays, Appl. Phys. Lett. 91 (2007), 181112.
[2] V.K. Tikhomirov, M. Mortier, P. Gredin, G. Patriarche, V.V. Moshchalkov, Preparation and up-conversion luminescence of 8 nm rare-earth doped fluoride nanoparticles, Opt. Express 16 (2008), 14544.
[3] V.D.R. FransZ, Henry S. LiT, Vail A.K. Raap, R.S. Niedbala, H.J. Tanke, Up-converting phosphor reporters for nucleic acid microarrays, Nat. Biotechnol. 19 (2001) 273–276.
[4] Y. Yang, Q. Shao, R. Deng, C. Wang, X. Teng, K. Cheng, Z. Cheng, L. Huang, Z. Liu, X. Liu, B. Xing, In vitro and in vivo uncaging and bioluminescence imaging by using photocaged upconversion nanoparticles, Angew. Chem. Int. Ed. Engl. 51 (2012) 3125–3129.
[5] L. Lu, D. Tu, Y. Liu, S. Zhou, W. Zheng, X. Chen, Ultrasensitive detection of cancer biomarker microRNA by amplification of fluorescence of lanthanide nanoprobes, Nano Res. 11 (2017) 264–273.
[6] W. Zheng, P. Huang, D. Tu, E. Ma, H. Zhu, X. Chen, Lanthanide-doped upconversion nano-bioprobes: electronic structures, optical properties, and biodetection, Chem. Soc. Rev. 44 (2015) 1379–1415.
[7] F. Wang, X. Xue, X. Liu, Multicolor tuning of (Ln, P)-doped YVO4 nanoparticles by single-wavelength excitation, Angew. Chem. Int. Ed. Engl. 120 (2010) 920–923.
[8] Y. Liu, D. Wang, J. Shi, Q. Peng, Y. Li, Magnetic tuning of upconversion luminescence in lanthanide-doped bifunctional nanocrystals, Angew. Chem. Int. Ed. 125 (2013) 4466–4469.
[9] D. Hudry, I.A. Howard, R. Popescu, D. Gerthsen, B.S. Richards, Structure-property relationships in lanthanide-doped upconverting nanocrystals: recent advances in understanding core-shell structures, Adv. Mater. 31 (2019), 1900623.
[10] S. Han, R. Deng, X. Xie, X. Liu, Enhancing luminescence in lanthanide-doped upconversion nanoparticles, Angew. Chem. Int. Ed. Engl. 53 (2015) 11702–11715.
[11] C.F. Gainer, G.S. Joshua, C.D. Silva, M. Romanowski, Control of green and red upconversion in $NaYF_4$:Yb^{3+}, Er^{3+} nanoparticles by excitation modulation, J. Mater. Chem. 21 (2011) 18530–18533.
[12] V.K. Tikhomirov, L.F. Chibotaru, D. Saurel, P. Gredin, M. Mortier, V. V. Moshchalkov, Er^{3+}-doped nanoparticles for optical detection of magnetic field, Nano Lett. 9 (2009) 721–724.
[13] R. Deng, F. Qin, R. Chen, W. Huang, M. Hong, X. Liu, Temporal full-colour tuning through non-steady-state upconversion, Nat. Nanotechnol. 10 (2015) 237–242.
[14] C.F. Gainer, G.S. Joshua, C.R. De Silva, M. Romanowski, Control of green and red up-conversion in NaYF4:Yb^{3+}, Er^{3+}nanoparticles by excitation modulation, J. Mater. Chem. 21 (2011) 18530–18533.
[15] D. Tu, L. Liu, Q. Ju, Y. Liu, H. Zhu, R. Li, X. Chen, Time-resolved FRET biosensor based on amine-functionalized lanthanide-doped $NaYF_4$ nanocrystals, Angew. Chem. Int. Ed. Engl. 50 (2011) 6306–6310.
[16] H. Dong, L.D. Sun, C.H. Yan, Energy transfer in lanthanide upconversion studies for extended optical applications, Chem. Soc. Rev. 44 (2015) 1608–1634.
[17] K.V. Yumashev, I.A. Denisov, N.N. Posnov, P.V. Prokoshin, V.P. Mikhailov, Nonlinear absorption properties of Co^{2+}:$MgAl_2O_4$ crystal, Appl. Phys. B 70 (2000) 179–184.
[18] S. Xu, W. Wang, S. Zhu, B. Zhu, J. Qiu, Highly efficient red, green and blue upconversion luminescence of Eu^{3+}/Tb^{3+}-codoped silicate by femtosecond laser irradiation, Chem. Phys. Lett. 442 (2007) 492–495.
[19] L. Sun, A. Li, F. Guo, Q. Lü, Y. Xu, L. Zhao, Enhanced 1.5μm emission and simultaneously suppressed green upconversion emission in Er:$LiNbO_3$ crystals heavily codoped with MgO, Appl. Phys. Lett. 91 (2007), 71914.
[20] A. Li, L. Sun, Z. Zheng, W. Wu, W. Liu, Y. Yang, T. Lü, W. Su, Spectroscopic analysis of Er^{3+} transition in Mg/Er-codoped $LiNbO_3$ crystal, J. Lumin. 128 (2008) 239–244.
[21] L. Li, Z. Zhou, H. Tian, D. Gong, Z. Yang, Y. Yang, Spectroscopic and upconversion properties of erbium-doped potassium lithium tantalate niobate crystals under 800 nm femtosecond laser excitation, J. Appl. Phys. 108 (2010), 043520.
[22] X. Shang, P. Chen, W. Cheng, K. Zhou, J. Ma, D. Feng, S. Zhang, Z. Sun, J. Qiu, T. Jia, Fine tunable red-green upconversion luminescence from glass ceramic containing 5%Er^{3+}:$NaYF_4$ nanocrystals under excitation of two near infrared femtosecond lasers, J. Appl. Phys. 116 (2014), 63110.
[23] Y. Yao, C. Xu, Y. Zheng, C. Yang, P. Liu, T. Jia, J. Qiu, Z. Sun, S. Zhang, Femtosecond laser-induced upconversion luminescence in rare-earth ions by nonresonant multiphoton absorption, J. Phys. Chem. A 120 (2016) 5522–5526.
[24] A. Li, Z. Zheng, T. Lü, Q. Lü, W. Liu, Red upconversion emission in $LiNbO_3$ codoped with Er^{3+} and Eu^{3+}, Opt. Express 17 (2009) 3878–3883.
[25] S. Zhang, Y. Yao, S. Xu, P. Liu, J. Ding, T. Jia, J. Qiu, Z. Sun, Realizing up-conversion fluorescence tuning in lanthanide-doped nanocrystals by femtosecond pulse shaping method, Sci. Rep. 5 (2015), 13337.
[26] L.Z. Deng, Y. Yao, L. Deng, H. Jia, Y. Zheng, C. Xu, J. Li, T. Jia, J. Qiu, Z. Sun, S. Zhang, Tuning up-conversion luminescence in Er^{3+}-doped glass ceramic by phase-shaped femtosecond laser field with optimal feedback control, Front. Physiol. 14 (2019), 13602.
[27] Y. Zheng, L. Deng, J. Li, T. Jia, J. Qiu, Z. Sun, S. Zhang, Controlling multiphoton excited energy transfer from Tm^{3+} to Yb^{3+} ions by a phase-shaped femtosecond laser field, Photon. Res. 7 (2019) 486–492.
[28] Y. Yao, C. Xu, Y. Zheng, C. Yang, P. Liu, J. Ding, T. Jia, J. Qiu, S. Zhang, Z. Sun, Improving upconversion luminescence efficiency in Er^{3+}-doped $NaYF_4$ nanocrystals by two-color laser field, J. Mater. Sci. 51 (2016) 5460–5468.
[29] M. Pollnau, D.R. Gamelin, S. Lüthi, H. Güdel, M.P. Hehlen, Power dependence of upconversion luminescence in lanthanide and transition-metal-ion systems, Phys. Rev. B 61 (2000) 3337–3346.
[30] W. Luo, C. Fu, R. Li, Y. Liu, H. Zhu, X. Chen, Er^{3+}-doped anatase TiO_2 nanocrystals: crystal-field levels, excited-state dynamics, upconversion, and defect luminescence, Small 7 (2011) 3046–3056.
[31] Y. Liu, X. Liu, W. Wang, T. Yu, Q. Zhang, Intense 2.7mm mid-infrared emission of Er^{3+} in oxyfluoride glass ceramic containing $NaYF_4$ nanocrystals, Mater. Res. Bull. 76 (2016) 305–310.
[32] Y. Liu, X. Liu, W. Wang, B. Zhou, Q. Zhang, Effect of adjusting composition on the crystallization and luminescence properties in $NaYF_4$:Er^{3+} embedded glass ceramics, Mater. Res. Bull. 95 (2017) 235–242.
[33] C. Hu, Z. Wu, X. Yang, W. Zhao, C. Ma, M. Chen, P. Xi, H. Chen, MUTE-SIM: multiphoton up-conversion time-encoded structured illumination microscopy, OSA Continuum 3 (2020) 594–608.
[34] C. Liu, W. Liu, S. Wang, H. Li, Z. Lv, F. Zhang, D. Zhang, J. Teng, T. Zheng, D. Li, M. Zhang, P. Xu, Q. Gong, Super-resolution nanoscopy by coherent control on nanoparticle emission, Sci. Adv. 6 (eaaw6579) (2020) 1–8.
[35] N. Dudovich, B. Dayan, S.G. Faeder, Y. Silberberg, Transform-limited pulses are not optimal for resonant multiphoton transitions, Phys. Rev. Lett. 86 (2001) 47–50.